THE JOURNAL OF COMPARATIVE NEUROLOGY 329:20–35 (1993)

The Projections of Intracellularly Labeled Auditory Nerve Fibers to the Dorsal Cochlear Nucleus of Cats

DAVID K. RYUGO AND SARAH K. MAY
Center for Hearing Sciences, Departments of Otolaryngology-Head and Neck Surgery and Neuroscience, Johns Hopkins University School of Medicine, Baltimore, Maryland 21205

ABSTRACT

The cochlear nucleus receives incoming auditory nerve discharges, preserves or transforms the signals, and distributes outgoing activity to higher centers. The organization of auditory nerve input to the cochlear nucleus will heavily influence the mechanisms by which acoustic information is processed. In order to study structure-function relationships between auditory nerve and cochlear nucleus, the axonal arborizations of type I spiral ganglion cells were labeled with intracellular injections of horseradish peroxidase after first being electrophysiologically characterized by recording with a micropipette inserted into the axon. For each auditory nerve fiber, spontaneous discharge rate (SR) and a frequency tuning curve were determined. The tuning curve yielded the characteristic frequency (CF, that frequency to which the fiber is most sensitive) and CF threshold in dB SPL. Individual axonal arborizations including all terminal swellings were reconstructed through serial sections with the aid of a light microscope and drawing tube. On average, 13.4 ± 8.1% of the terminal swellings were found in the dorsal cochlear nucleus (DCN) and the remaining terminal swellings were located in the ventral cochlear nucleus. In the DCN, the terminal fields of auditory nerve fibers were restricted to layer III, contributed to cytoarchitectonic striations, and exhibited a systematic relationship between fiber CF and position along the strial (or long) axis of the nucleus. Computer-aided rotations revealed that the terminal fields were anisotropic, being flattened within the trans-strial axis. The maximal width of the terminal fields along the strial axis ranged from 31–321 μm and was inversely related to fiber CF and SR. Variation in the number of terminals or depth of the terminal field within layer III was not related to SR grouping or CF of the fiber.

Key words: hearing, horseradish peroxidase, primary sensory neurons, tonotopy, topography

The auditory nerve conducts information from the cochlear receptors into the cochlear nucleus. The cochlear nucleus is not only the first site for the central processing of acoustic information, but also the origin of neural circuits comprising the ascending auditory pathways. The cochlear nucleus has two major divisions, the dorsal (DCN) and the ventral (VCN) cochlear nuclei. Each division contains distinct populations of cell types and has a characteristic internal organization. The DCN is a laminated cortical structure, whereas the VCN is not (e.g., Rámon y Cajal, '09; Osen, '69; Mugnaini et al., '80; Lorente de No, '81). Not surprisingly, the two divisions manifest definable differences in electrophysiological response properties (e.g., Pfeiffer, '66; Evans and Nelson, '73; Goldberg and Brownell, '73) react differently to cochlear destruction (Koerber et al., '66) and are distinguishable by their axonal projections to higher auditory centers (e.g., Warr, '82). The VCN has been proposed as having a role in eliciting the acoustic middle ear muscle reflex (Borg, '73), in mediating the acoustic startle response (Davis et al., '82), and in processing time and intensity cues for sound localization (Young et al., '88). In contrast, little is known about the function of the DCN, a circumstance that is highlighted by puzzling anatomical singularities evident in "specialized" mammals such as bats (Feng and Vater, '85) and primates (Moore, '80). Our working hypothesis is that clues fundamental to understanding coding mechanisms in the DCN are embedded in features of the organization of auditory nerve input.

In this context, we have been studying the axonal arborizations of single auditory nerve fibers into the DCN. The

Accepted November 3, 1992.

Address reprint requests to D.K. Ryugo, Center for Hearing Sciences, Johns Hopkins University School of Medicine, Traylor Research Building, Room 510, 720 Rutland Avenue, Baltimore, MD 21205.

Dr. S.K. May is now at the Department of Medicine, Boston City Hospital, Thorndike Building, 3rd Floor, 818 Harrison Avenue, Boston, MA 02118.

projection of a population of auditory nerve fibers into the cochlear nucleus has been previously determined by mapping the distribution of degeneration following partial cochlear ablations (Sando, '65; Osen, '70; Webster, '71; Moskowitz and Liu, '72; Noda and Pirsig, '74) or by plotting the location of labeled axons and terminals following horseradish peroxidase (HRP) injections into the spiral ganglion (Leake and Snyder, '89; Brown and Ledwith, '90). Analysis of primary projections at the single fiber level not only provides important information with much greater resolution but also remains an important adjunct to cellular and ultrastructural studies in the DCN (Rhode et al., '83; Wouterlood et al., '84; Wouterlood and Mugnaini, '84; Mugnaini, '85; Smith and Rhode, '85; Mugnaini et al., '87). For example, pyramidal cells of the DCN exhibit basal dendrites that are flattened within the frequency plane (Blackstad et al., '84; Ryugo and Willard, '85). The basal dendrites of pyramidal cells are one of the targets of primary fibers arising from the cochlea (Kane, '74; Smith and Rhode, '85), and we sought to investigate the terminations of these fibers in relation to the dendritic planes. We also studied whether fibers of different characteristic frequency (CF) or spontaneous rate (SR) groups exhibited different termination patterns.

In the present study, the response properties of individual auditory nerve fibers were recorded prior to intracellular staining. For each fiber, the characteristics of the projection, the axonal arborization, and the size, shape, and spatial location of terminal swellings were examined. These structural features were then considered with respect to the fiber's physiological properties.

MATERIALS AND METHODS

Physiology and histology

In this study, a total of 22 cats of either sex, weighing between 1.5 and 3 kg, and free of middle ear infections were used. Surgical procedures, the means of delivering acoustic stimuli, and techniques for recording and processing single unit data have been previously described (Kiang et al., '65; Liberman, '78). Details for intracellular recording, HRP injections, histological procedures, and recovery of labeled fibers have also been described (Fekete et al., '84; Rouiller et al., '86). Briefly, animals were anesthetized with intraperitoneal injections of dial-urethane (0.5 cc per kg) (where each cc contains 100 mg of Diallyl barbituric acid, 400 mg of Urethane, and 400 mg of ethylurea). Supplemental doses were administered in order to maintain areflexia to paw pinches. The skin and muscle layers overlying the skull were removed. The bulla was opened to allow for round window recordings and the external meati were cut just peripheral to the tympanic ring to allow insertion of the acoustic system. The posterior fossa was opened with rongeurs, the dura reflected over the cerebellum, and the cerebellum retracted to expose the auditory nerve between the internal auditory meatus and the cochlear nucleus. Recording micropipettes were then placed into the nerve under direct visual control with the aid of an operating microscope.

For each unit, a threshold tuning curve and a 15-second period of spontaneous activity (SR) were obtained before and after the injection of HRP. The similarity of pre- and post-injection response features and the continuously negative DC potential provide evidence that the injected fiber was the same one from which recordings were obtained. The tuning curve was used to determine CF, that pure tone frequency to which the unit was most sensitive. SR was defined as spike activity (spikes per second, s/s) in the absence of sound controlled by the investigator. Units are assigned to SR groups by using the criterion of Liberman ('78): low SR < 0.5 s/s, medium SR = 0.5–18 s/s, and high SR > 18 s/s). Low and medium SR fibers were sometimes grouped together for comparisons with high SR fibers because they share a number of common features (Evans and Palmer, '80; Liberman, '82a; Fekete et al., '84; Ryugo and Rouiller, '88; Ryugo and Sento, '91). Individual fibers were intracellularly marked by iontophoresing a 10% solution of HRP (Sigma type VI) in 0.05 M Tris buffer (pH 7.3) containing 0.15 M KCl through micropipettes bevelled to a final impedance of 40–60 MΩ. Approximately 24 hours after the HRP injection, the cat was given a lethal dose of barbiturate, artificially respired, and perfused through the heart with 50 cc of isotonic saline (37°C) with 0.1% $NaNO_2$ in 0.12 M cacodylate buffer (pH 7.4), followed immediately by 500 ml of warm (37°C) fixative containing 0.5% paraformaldehyde, 1% glutaraldehyde, and 0.008% $CaCl_2$ in 0.12 M cacodylate buffer (pH 7.4), and then by 1.5 L of a second fixative containing 1.25% paraformaldehyde, 3% glutaraldehyde, and 0.008% $CaCl_2$ in the same buffer solution. Following perfusion and decapitation, the head was immersed in the second fixative (5°C) overnight. Then, the brain was removed from the skull and the auditory nerve, cochlear nucleus, and adjacent brainstem isolated in a single tissue block. The two sides of the brain were typically processed separately so that sections could be taken approximately parallel to the dorsolateral surface of the cochlear nucleus (see Fig. 2 of Fekete et al., '84). In three cases, the brain was sectioned in the transverse plane.

Each tissue block was embedded in a gelatin-albumin mixture hardened with glutaraldehyde, cut into 50 μm thick sections on a Vibratome, and kept in serial order. The sections were rinsed several times in 0.1 M Tris buffer (pH 7.6) prior to incubating for 1 hour in 0.5% $CoCl_2$ in Tris buffer. Sections were then rinsed in Tris buffer, rinsed again in 0.1 M phosphate buffer (pH 7.3), and incubated for 1 hour with 0.05% 3.3′-diaminobenzidine (DAB, Sigma grade II TetraHCl) in phosphate buffer. The tissue was reacted for an additional hour with a fresh solution of DAB to which was added 0.01% H_2O_2. After rinsing in phosphate buffer, tissue was mounted onto gelatin coated slides, air dried overnight, counterstained with 0.5% cresyl violet, and coverslipped in Permount.

Reconstructions of the cochlear nucleus

Anatomical atlases (×40 total magnification) were prepared from serial histological sections of cochlear nuclei with the aid of an overhead projector (Tri-simplex with a Zeiss lens). Ten nuclei from nine experimental cats were used. The Schwann-glia border acted as the boundary between auditory nerve and cochlear nucleus. Medially, the nucleus was bounded by fibers of the trigeminal and vestibular nerves, the inferior and middle cerebellar peduncles, and the acoustic striae. The boundary between the DCN and the VCN for each section was marked by the granule cell lamina and intermittent islets of granule cells. The DCN and VCN outlines were then aligned in series by using the cut edges of the tissue and histologic landmarks (such as blood vessels), and traced with the stylus of a graphics tablet in order to compute the area (excluding the above granule cell domain) for each section (SigmaScan,

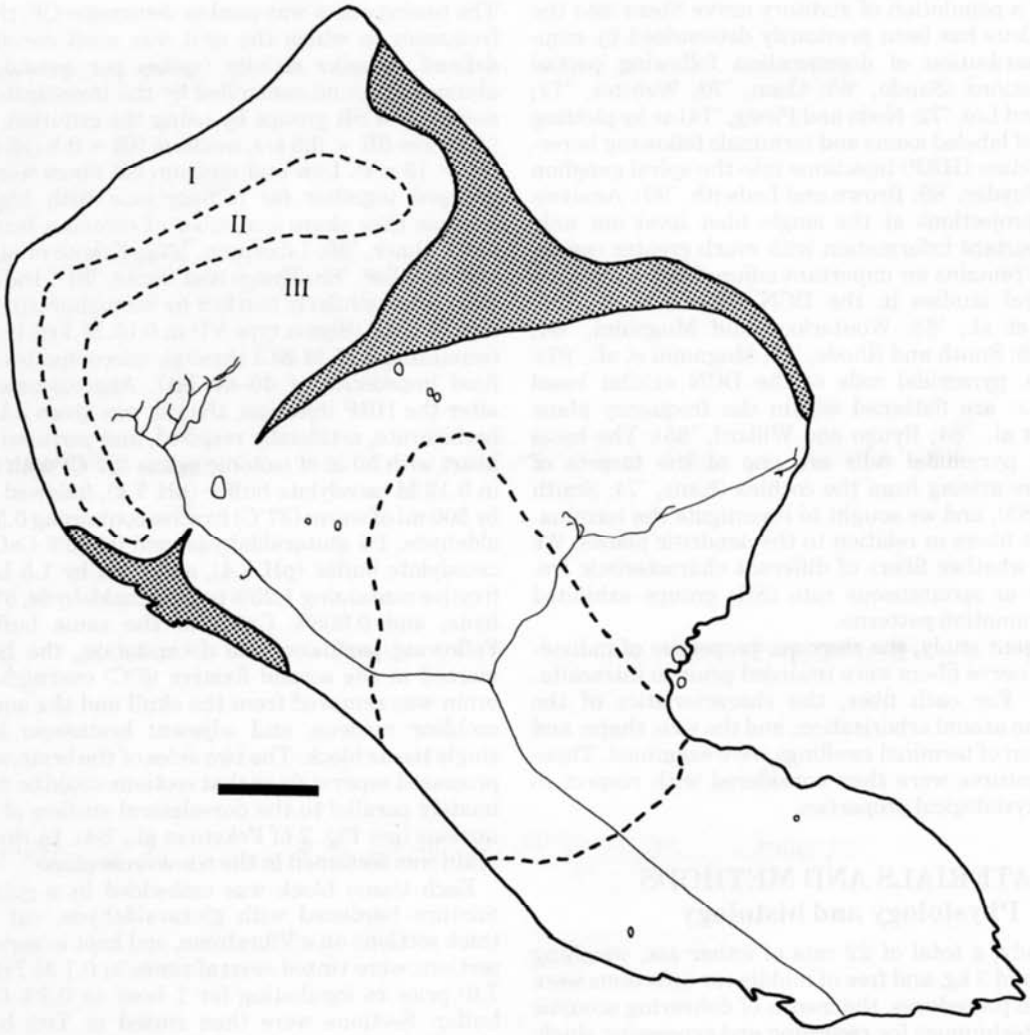

Fig. 1. Parasagittal view of the right cochlear nucleus. This figure illustrates the main trajectory of a type I auditory nerve fiber (CF = 0.82 kHz; SR = 56 s/s) within the nucleus, as reconstructed through serial sections with the aid of a light microscope and drawing tube. Note the arborization of the descending branch within layer III of the dorsal cochlear nucleus (DCN). Three of the DCN layers are marked with Roman numerals. Other features are labeled on the inset diagram of Figure 2. Stipple indicates granule cell domains. Anterior is to the right; dorsal is up. Scale bar = 0.5 mm.

Jandel Scientific). The tissue volume was calculated by multiplying each area by its corresponding section thickness. Total nuclear volume was defined as the sum of the sectional volumes. Terminal fields were also plotted on these sections, and their absolute and relative positions along the strial axis calculated.

Reconstructions of fibers and endings

Single fibers were reconstructed from serial sections at a total magnification of ×312 with the aid of a light microscope and drawing tube. Labeled fiber segments were pieced together by aligning cut ends and blood vessels on the surfaces of adjacent tissue sections. The entire descending branch as it entered the DCN and all primary collaterals within the VCN were drawn at a total magnification of ×1250. Counts of terminal swellings and measurements of silhouette area were conducted from these high magnification drawings. Area measurements were determined with the aid of the graphics tablet.

The location of the geometric center of the endbulbs in the anteroventral cochlear nucleus (AVCN) and of the terminal fields in the DCN was determined from the planar projections of each fiber onto the silhouette of its nucleus. The maximal dorsal-to-ventral distance of the anterior division of the AVCN (taken perpendicular to the trajectory of the ascending branch) and of layer II (along the strial axis) in the DCN was used as the denominator, and the distance from the ventral border of the nucleus to the appropriate ending was placed in the numerator; the resulting percentage was used to represent the normalized position of the ending.

Computer-aided graphics system

Our computerized imaging system (Neurotrace System, Interactions Co., Cambridge, MA) enabled points (branch points, en passant swellings, and terminal swellings) and lines (axon segments) to be entered with the aid of a light microscope. The software utilized a calibrated mouse for

Fig. 2. Photomontage of a parasagittal section of the right cochlear nucleus. This micrograph illustrates the cellular striations of layer III in the DCN. Scale bar = 0.5 mm. Inset: diagram of micrograph showing striations within layer III. ANR, auditory nerve root; AVCN, anteroventral cochlear nucleus; DCN, dorsal cochlear nucleus; PVCN, posteroventral cochlear nucleus; sgb, Schwann-glia border.

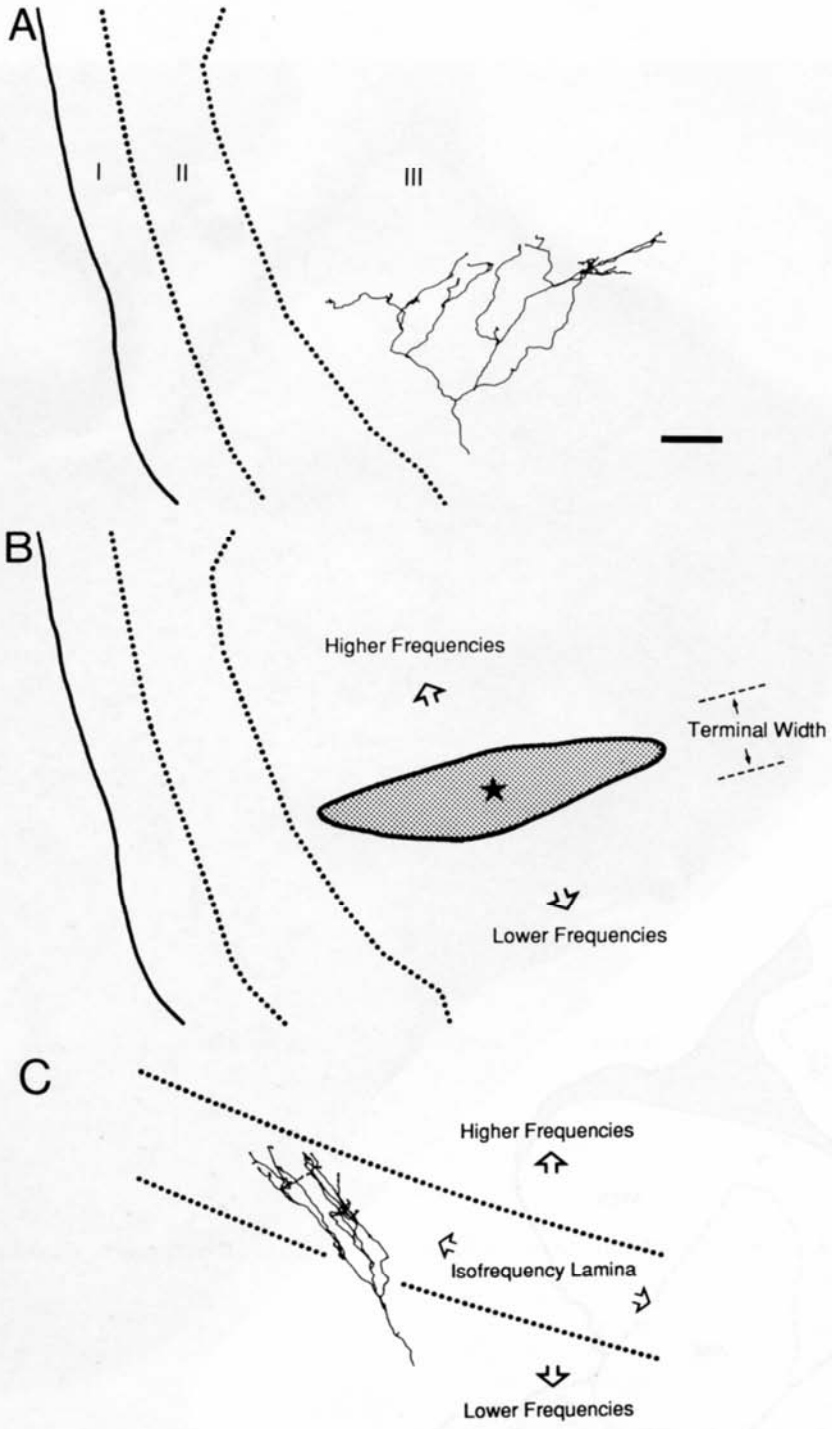

Fig. 3. Computer-assisted illustration of HRP-labeled, high spontaneous discharge rate (SR) auditory nerve fiber shown in Figure 1 (CF = 0.82 kHz; SR = 56 s/s). In panel **A**, the arborization is presented from a plane parallel to the lateral surface of the nucleus (modified parasagittal plane as illustrated in Fig. 2 of Fekete et al., '84) and shown to be confined to layer III. The terminal field is elongated within the depth of layer III, extending perpendicularly with respect to the ependymal surface. In panel **B**, the envelope (stipple) of the distribution of terminal swellings is shown as it lies in the frequency axis. The star indicates the geometric center of the arborization, and is used for this purpose in the insets of Figures 4–8. The terminal field width is compressed along the strial axis to define a relatively narrow frequency band. In panel **C**, the fiber has been rotated 90° to reveal its limited expansion within the isofrequency band of layer III. The narrow dimensions of this tube-like arborization suggest that a number of auditory nerve fibers must contribute to the isofrequency lamina. Scale bar = 100 μm for all panels.

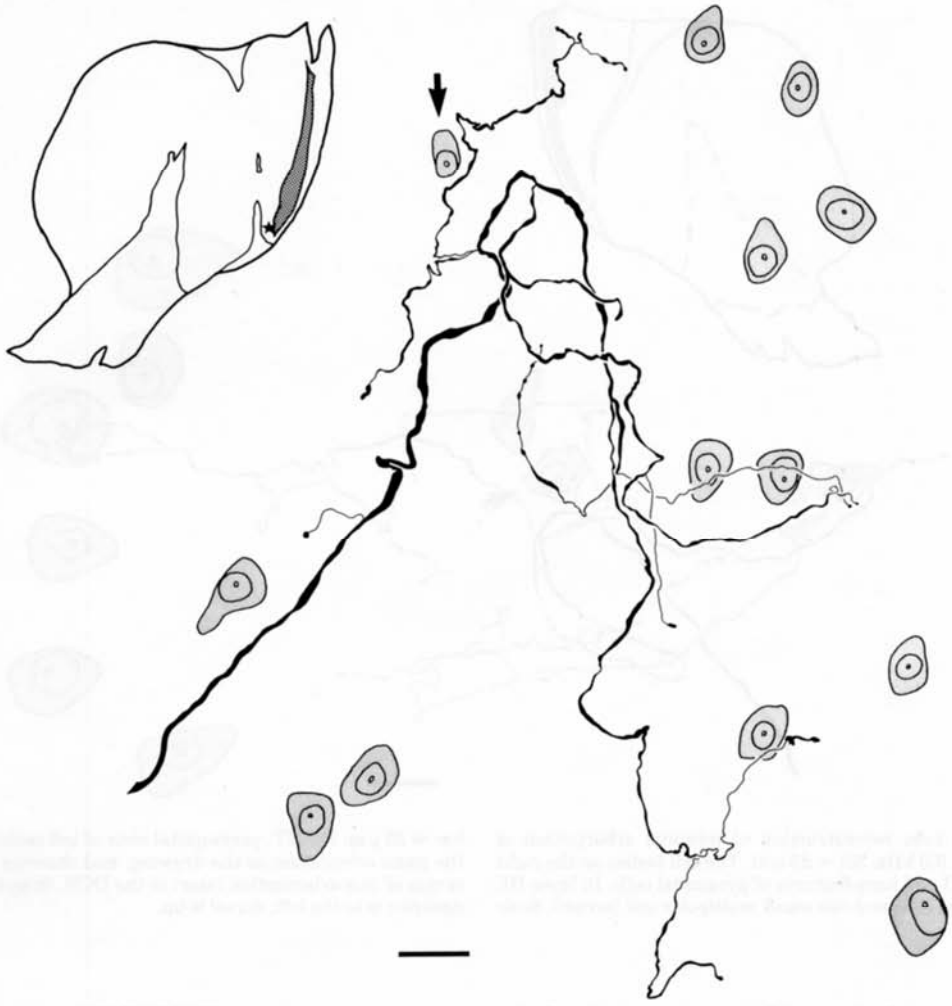

Fig. 4. Drawing tube reconstruction of terminal arborization of high SR fiber (CF = 0.55 kHz; SR = 63.5 s/s). Note the relatively narrow terminal field. All of the cell bodies have features of pyramidal cells except for the single vertical cell (arrow). Scale bar = 25 μm. INSET: parasagittal view of left cochlear nucleus having the same orientation as the drawing, and showing the location of the center of this arborization (star) in the DCN. Stipple indicates layer II. Anterior is to the left; dorsal is up.

entering the planar location (x,y) of a structure, and a position sensor attached to the fine focus control of the light microscope for entering the depth (z) of that structure. The image of the entered data was shown on a computer monitor and feedback was provided through the microscope oculars by way of a drawing tube. This system enabled us to reconstruct single axons at the highest optical magnifications while keeping track of locations within the subdivisions of the nucleus as defined in low power tracings. Entire individual axons complete with swellings could be displayed with or without regional boundaries that had been entered. Images could also be rotated and viewed from any angle.

Because we mounted hydrated tissue sections onto microscope slides prior to the dehydration and clearing steps, there was virtually no shrinkage of tissue in the x-y plane. We have determined, however, that there is approximately a 50% decrease in tissue thickness in the z plane. This determination was made immediately following HRP processing by embedding individual tissue sections "on end" in agar and then measuring using a calibrated micrometer. These measured values matched that determined from the fine focus of the microscope and Vibratome setting by ±8%. After histologic processing, measurements using the fine focus indicated that the section thickness decreased by 50%. Depth measurements have been doubled to compensate for such shrinkage; area values represent raw scores. Means, standard deviations, and P values (Student's t test, two-tailed) are provided where appropriate.

Counts of pyramidal cells

Pyramidal cells of the DCN were counted in two animals. In one case, cells were retrogradely labeled using HRP methods. A microliter syringe loaded with 30–40% HRP (Sigma Chemical Co., St. Louis, MO, type VI) in 0.1 M Tris buffer (pH 7.6) was mounted on a micromanipulator and advanced into the inferior colliculus in three sites, separated by several millimeters in the anterior-posterior direction. A total of 1 μL was injected along each track. Following a 24-hour survival, the animal was given a lethal dose of Nembutal and immediately perfused and prepared using the already mentioned procedures. Frontal, 50 μm

Fig. 5. Drawing tube reconstruction of terminal arborization of high SR fiber (CF = 6.0 kHz; SR = 53 s/s). The cell bodies on the right side reside in layer II and have features of pyramidal cells. In layer III, there are two vertical cells and one small multipolar cell (arrow). Scale bar = 25 μm. INSET: parasagittal view of left cochlear nucleus having the same orientation as the drawing, and showing the location of the center of this arborization (star) in the DCN. Stipple indicates layer II. Anterior is to the left; dorsal is up.

thick sections through the cochlear nucleus and inferior colliculus were serially mounted onto gelatin-coated slides and air-dried overnight. The next morning, tissue was soaked in a solution containing 0.02% benzidine dihydrochloride, 1% sodium nitroprusside, and 30% ethanol in 0.1 M acetate buffer (pH 5.0) for 30 minutes. Then the tissue was reacted in a fresh batch of the same solution containing 0.3% H_2O_2 for 20 minutes, stabilized in a solution containing 3% sodium nitroprusside and 50% ethanol in 0.1 M acetate buffer (pH 5.0), and counterstained with cresyl violet. This method was chosen because sections can be processed after they have been mounted on slides, thereby minimizing tissue distortion from dehydration without loss of histochemical sensitivity. Every HRP-labeled cell in layer II with a visible nucleus and nucleolus was counted in alternate sections. Microscopic analysis confirmed that the HRP injection site was restricted to and completely filled the inferior colliculus. In the other case, 50 μm thick sections from a normal cat were stained with cresyl violet. Every large cell in layer II exhibiting a pale-staining, round nucleus, a nucleolus, and prominent Nissl bodies in the cytoplasm was considered a pyramidal cell and counted in alternate sections. All raw counts were corrected for split-cell error by the Abercrombie ('46) correction, using the assumption that the nuclei were spherical [i.e., corrected count = (raw count × section thickness) divided by (section thickness + nuclear diameter)].

RESULTS

The axonal arborizations for this report are derived from 41 auditory nerve fibers in 23 cochlear nuclei from 20 cats. Twenty-four of these fibers were completely stained; an additional ten ascending branches and seven descending branches were analyzed. Six descending branches were excluded from this study because they did not enter the DCN but rather terminated in the posteroventral cochlear nucleus (PVCN).

The completeness of staining for any particular fiber was inferred from the observation that all collateral branches were darkly labeled with HRP reaction product, that there was no sign of progressive lightening of the reaction product with additional distance from the injection site, and that each collateral was marked by a terminal swelling. Twenty-six completely stained descending branches were digitized and entered into our computer system for analysis of their three-dimensional spatial orientation in the DCN. Attention was also given to features of the ascending and descending branch of the same fiber where possible.

Nuclear volume

The terminus of auditory nerve fibers is the cochlear nucleus. The ventral cochlear nucleus (VCN) is a structure somewhat flattened against the side of the brainstem and contains the auditory nerve root; the dorsal cochlear nucleus (DCN) is tubular in shape and resides dorsally and

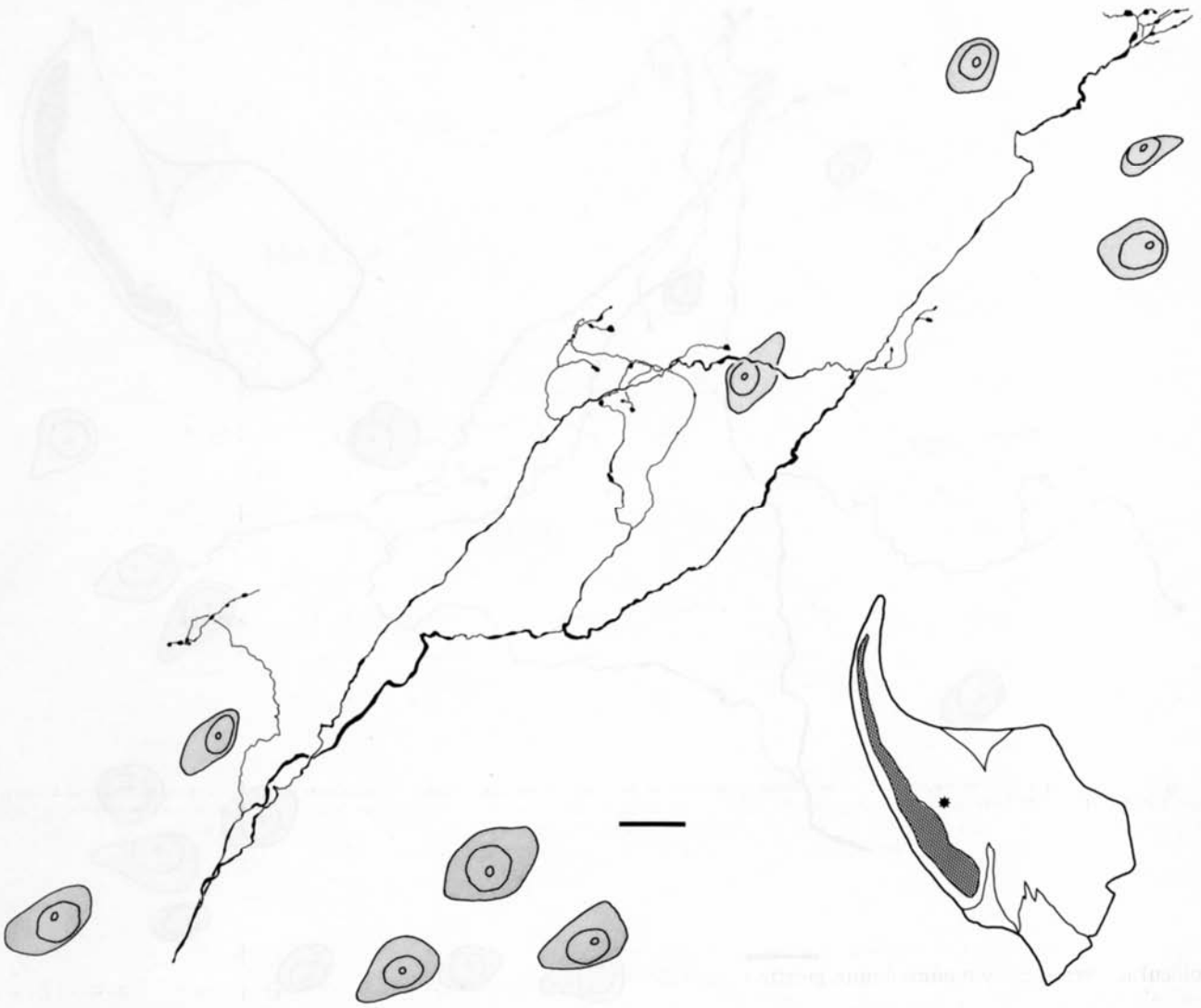

Fig. 6. Drawing tube reconstruction of terminal arborization of high SR fiber (CF = 11.2 kHz; SR = 19 s/s). The cell bodies in the lower left of the drawing are located in layer II and have features of pyramidal cells. In layer III, there are two vertical cells and two small multipolar cells. Scale bar = 25 μm. INSET: parasagittal view of right cochlear nucleus having the same orientation as the drawing, and showing the location of the center of this arborization (star) in the DCN. Anterior is to the right; dorsal is up. Stipple indicates layer II.

caudally with respect to the VCN, draping over its posterior aspect (see Fig. 1 of Blackstad et al., '84). The boundary between the DCN and the VCN is formed by an incomplete layer of granule cells (Mugnaini et al., '80). Volume calculations for each nucleus were made in order to determine the relative size relationships between structures. On average (±SD), the VCN comprised 18.7 ± 3.2 mm^3, whereas the DCN comprised 6.9 ± 1.2 mm^3. The DCN occupied 26.4 ± 3.1% of the total nuclear volume.

Fiber Morphology

Each fiber entered the cochlear nucleus ventrally from the auditory nerve, traveled a variable distance beyond the Schwann-glia border depending on its characteristic frequency (CF), and then bifurcated (Fig. 1). This particular fiber (CF = 0.82 kHz; SR = 56 s/s) was reconstructed at a total magnification of ×312 using a light microscope and drawing tube, and it demonstrates some of the representative attributes of type I auditory nerve fibers. The bifurcation is an obvious feature and gives rise to two major branches. The ascending branch projects anteriorly through the AVCN prior to forming the characteristic endbulb of Held, and the descending branch projects through the PVCN and usually (85% of the time) enters the DCN. Both ascending and descending branches give rise to collaterals along their course.

Terminal arborization in the DCN. Once the descending branch enters the DCN, it usually does not emit any collaterals until the emergence of the terminal arborization. Each terminal arborization appears as a tuft at the end of the descending branch and consists of a variable number of fairly localized branches. Although the arborizations were confined primarily within layer III, deep pyramidal cells were frequently in the vicinity and occasionally in direct apposition to terminal swellings. Layer III represents the superficial region of what has been known as the deep

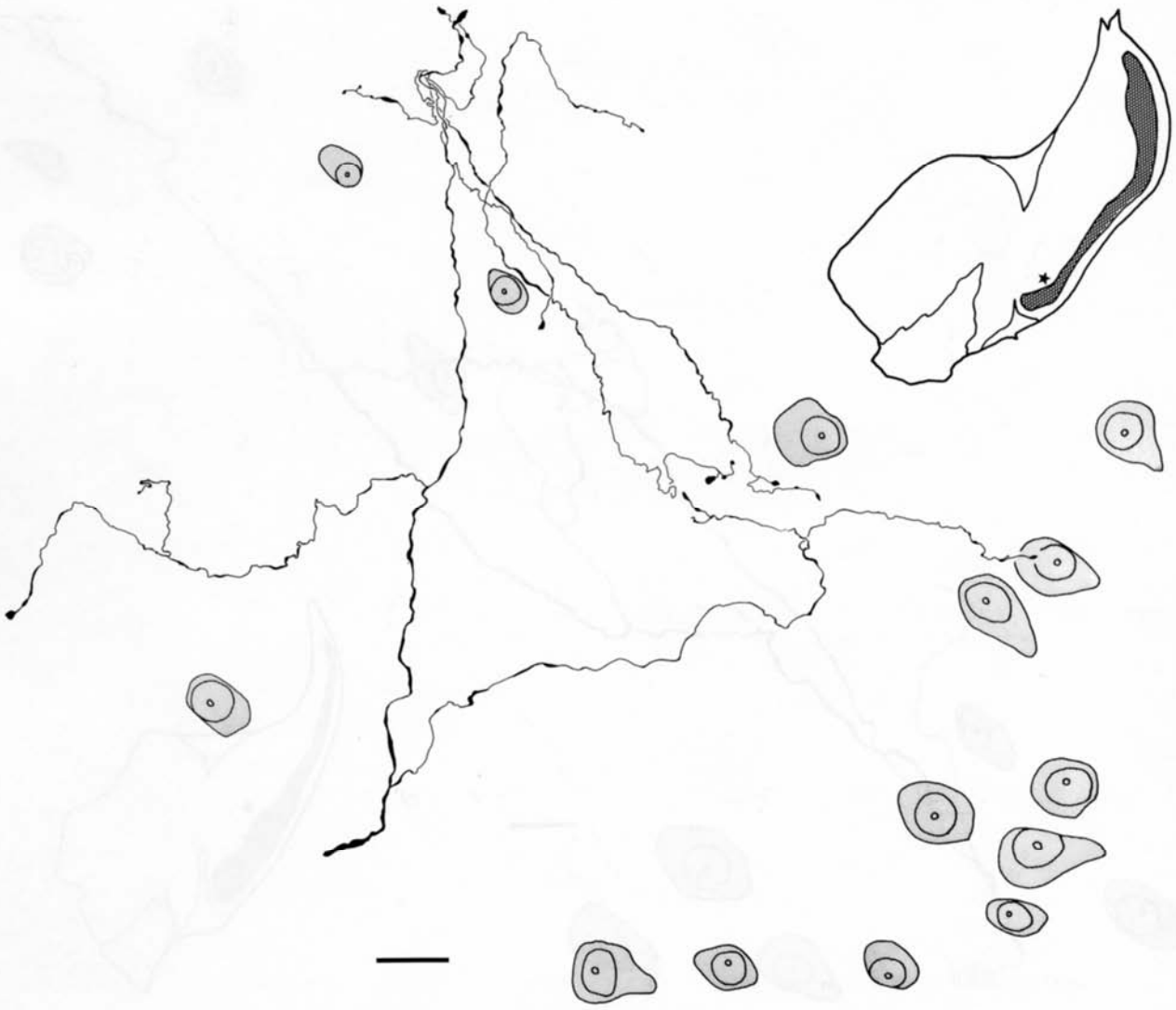

Fig. 7. Drawing tube reconstruction of terminal arborization of medium SR fiber (CF = 1.2 kHz; SR = 1 s/s). The cell bodies on the bottom and right side of the drawing are located in layer II and have features of pyramidal cells. In layer III, there are two small vertical cells. Scale bar = 25 μm. INSET: parasagittal view of left cochlear nucleus having the same orientation as the drawing, and showing the location of the center of this arborization (star) in the DCN. Anterior is to the left; dorsal is up. Stipple indicates layer II.

polymorphic layer. It is characterized by the presence of basal dendrites of overlying pyramidal cells, a lower cell density than layer II, and striations of cell bodies and fibers oriented perpendicularly to the ependymal surface (Fig. 2). Layer IV, the basal region of the deep polymorphic layer, is marked by a rich plexus of fibers.

Arborizations of fibers were also reconstructed at a higher magnification (×1,250) using a computer-aided system as well as a drawing tube. The advantage of computer tracings was that images could be rotated to any predetermined angle about any designated axis or axes while preserving the three-dimensional relationships of all structures. This computerized system assisted our descriptions of the spatial arrangement of terminal swellings. Individual terminal arborizations could be grouped into one of two patterns. One pattern of arborizations defines a relatively restricted cluster of terminal swellings (Fig. 3A). The distribution of the swellings forms a spatially elongated envelope whose long axis runs perpendicular to the ependymal surface between layers II and IV, and whose short axis (measured as the maximum excursion perpendicular to the long axis of the envelope) represents the width of what we have defined as an isofrequency lamina (Fig. 3B). The long axis of these arborizations within layer III ranged from 50–444 μm. When this "tube-shaped" arborization is rotated 90° and viewed "on edge," it is apparent that multiple auditory nerve fibers must contribute to an isofrequency lamina because no single arborization is sufficiently broad (Fig. 3C). Despite considerable variability in the branching pattern of individual fibers, even within the same animal, all high SR fibers (and a few low-medium SR fibers) exhibited this tight distribution of terminal swellings (Figs. 4–6). The other pattern of arborizations exhibits a spatially more dispersed terminal field (Figs. 7, 8). There is a

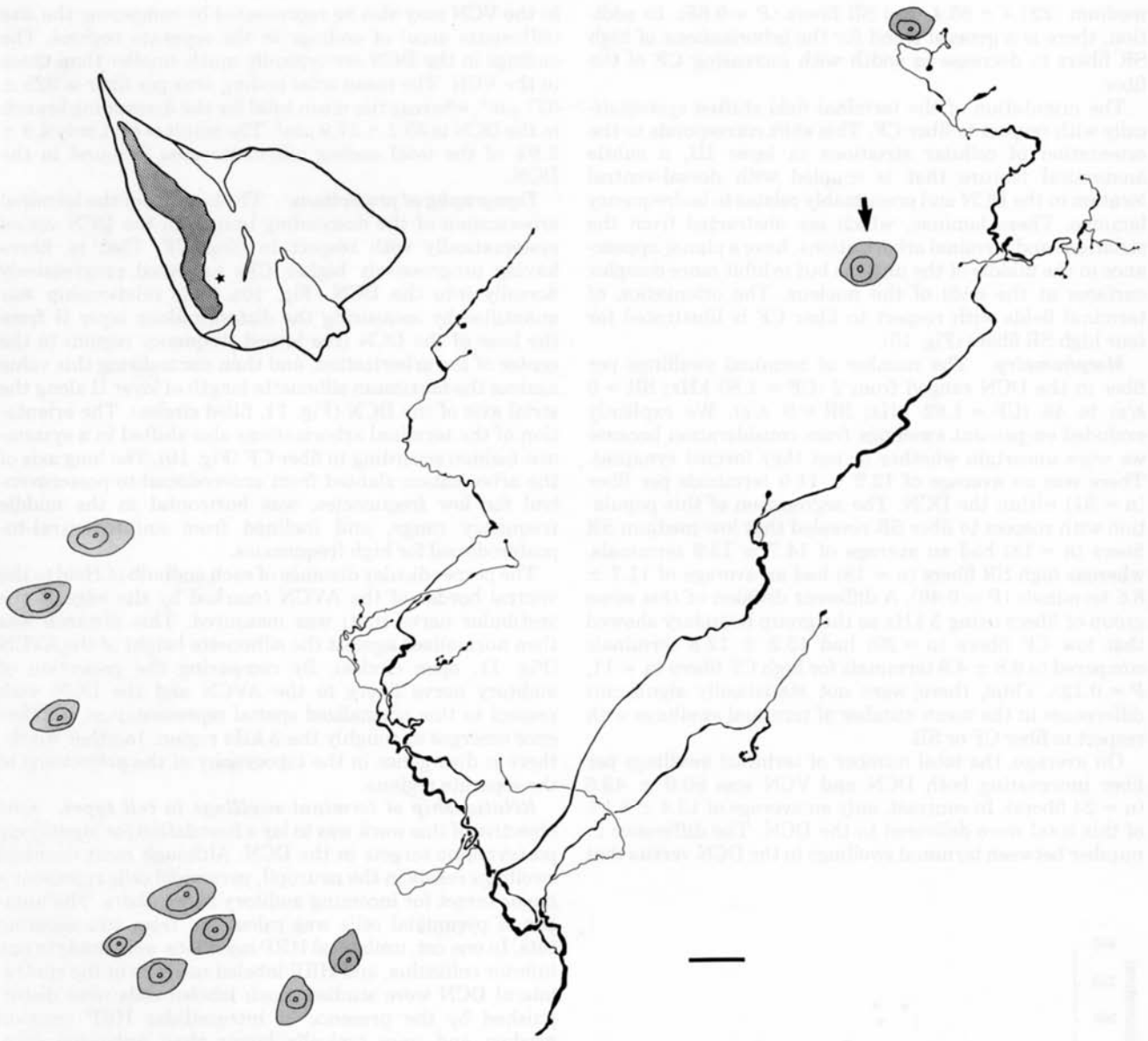

Fig. 8. Drawing tube reconstruction of terminal arborization of low SR fiber (CF = 3.1 kHz; SR = 0.2 s/s). The cell bodies on the lower left side of the drawing are located in layer II and have features of pyramidal cells. In layer III, there is a small multipolar cell and a giant cell (arrow). Scale bar = 25 μm. INSET: parasagittal view of right cochlear nucleus having the same orientation as the drawing, and showing the location of the center of this arborization (star) in the DCN. Anterior is to the right; dorsal is up. Stipple indicates layer II.

tendency for two clusters of terminals to be formed, separated by approximately 100–300 μm. These clusters could be distributed along the strial axis (Fig. 7) or within the depth of layer III (Fig. 8).

These drawing tube reconstructions illustrate the terminal arborizations and emphasize that nearly all swellings are located in the neuropil. Only an occasional superficial swelling approaches a pyramidal cell body. The remaining swellings presumably synapse on the dendrites of deeper-lying neurons, in addition to the basal dendrites of pyramidal cells. Two other populations of cells are found in the vicinity of labeled swellings and were categorized on the basis of their somatic size, shape, and staining characteristics: elongated cells (12–15 × 25–30 μm in diameter) with a centrally placed, round nucleus and diffusely staining cytoplasm, and multipolar cells (20–35 μm in diameter) with an eccentrically placed, round nucleus and blotchy-staining cytoplasm. These neuronal categories may be further subdivided but more analyses remain to be done.

The width of both patterns of terminal arborizations could be represented by the value of the maximal distance between terminals along the strial or frequency axis (Fig. 9). The average width of high SR fibers was 87.2 ± 40.6 μm, whereas that for low-medium SR fibers was 230.5 ± 72.8 μm ($P < 0.01$). There was no difference in terminal field width between the low SR fibers (244.3 ± 62.3 μm) and the

medium (221.4 ± 83.4 μm) SR fibers ($P = 0.65$). In addition, there is a general trend for the arborizations of high SR fibers to decrease in width with increasing CF of the fiber.

The orientation of the terminal field shifted systematically with respect to fiber CF. This shift corresponds to the orientation of cellular striations in layer III, a subtle anatomical feature that is coupled with dorsal-ventral location in the DCN and presumably relates to isofrequency laminae. These laminae, which are abstracted from the striations and terminal arborizations, have a planar appearance in the middle of the nucleus but exhibit more complex surfaces at the ends of the nucleus. The orientation of terminal fields with respect to fiber CF is illustrated for four high SR fibers (Fig. 10).

Morphometry. The number of terminal swellings per fiber in the DCN ranged from 2 (CF = 1.85 kHz; SR = 0 s/s) to 48 (CF = 1.82 kHz; SR = 0 s/s). We explicitly excluded en passant swellings from consideration because we were uncertain whether or not they formed synapses. There was an average of 12.9 ± 11.0 terminals per fiber (n = 31) within the DCN. The segregation of this population with respect to fiber SR revealed that low-medium SR fibers (n = 13) had an average of 14.7 ± 13.9 terminals, whereas high SR fibers (n = 18) had an average of 11.7 ± 8.6 terminals ($P = 0.46$). A different division of this same group of fibers using 5 kHz as the group boundary showed that low CF fibers (n = 20) had 15.2 ± 12.8 terminals compared to 8.8 ± 4.8 terminals for high CF fibers (n = 11, $P = 0.12$). Thus, there were not statistically significant differences in the mean number of terminal swellings with respect to fiber CF or SR.

On average, the total number of terminal swellings per fiber innervating both DCN and VCN was 80.6 ± 43.6 (n = 24 fibers). In contrast, only an average of 13.4 ± 8.1% of this total were delivered to the DCN. The difference in number between terminal swellings in the DCN versus that in the VCN may also be represented by comparing the size (silhouette area) of endings in the separate regions. The endings in the DCN are typically much smaller than those in the VCN. The mean total ending area per fiber is 825 ± 327 μm^2, whereas the mean total for the descending branch in the DCN is 35.2 ± 27.9 μm^2. The result is that only 4.3 ± 2.8% of the total ending silhouette area is found in the DCN.

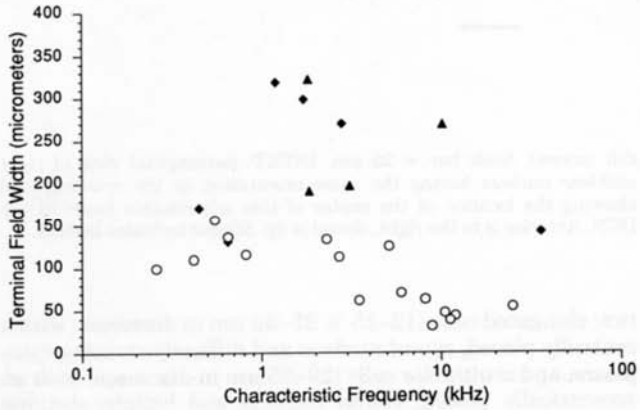

Fig. 9. Scatter plot illustrating the relationship between fiber CF and maximum terminal field width as measured along the strial axis (n = 26 descending branches). High SR fibers are represented by open circles, medium SR fibers by filled diamonds, and low SR fibers by filled triangles. Note that the widths of the terminal fields of high SR fibers are narrower than those of low-medium SR fibers. Although the sample size is small, it seems that the terminal field width for high SR fibers is inversely related to fiber CF.

Topography of projections. The location of the terminal arborization of the descending branch in the DCN varied systematically with respect to fiber CF. That is, fibers having progressively higher CFs projected progressively dorsally into the DCN (Fig. 10). This relationship was quantified by measuring the distance along layer II from the base of the DCN (the lowest frequency region) to the center of the arborization, and then normalizing this value against the maximum silhouette length of layer II along the strial axis of the DCN (Fig. 11, filled circles). The orientation of the terminal arborizations also shifted in a systematic fashion according to fiber CF (Fig. 10). The long axis of the arborization slanted from anterodorsal-to-posteroventral for low frequencies, was horizontal in the middle frequency range, and inclined from anteroventral-to-posterodorsal for high frequencies.

The perpendicular distance of each endbulb of Held to the ventral border of the AVCN (marked by the edge of the vestibular nerve root) was measured. This distance was then normalized against the silhouette height of the AVCN (Fig. 11, open circles). By comparing the projection of auditory nerve fibers to the AVCN and the DCN with respect to this normalized spatial representation, a difference emerges at roughly the 3 kHz region. In other words, there is divergence in the topography of the projections to the separate regions.

Relationship of terminal swellings to cell types. One objective of this work was to lay a foundation for identifying postsynaptic targets in the DCN. Although most terminal swellings reside in the neuropil, pyramidal cells represent a major target for incoming auditory nerve fibers. The number of pyramidal cells was calculated from two separate cats. In one cat, unilateral HRP injections were made in one inferior colliculus, and HRP-labeled neurons in the contralateral DCN were studied. Such labeled cells were distinguished by the presence of intracellular HRP reaction product and were typically larger than unlabeled ones. Their distribution in the DCN was consistent with that described for pyramidal and giant cells (Osen, '69; Adams and Warr, '76). Within layer II, labeled cells were identified as pyramidal cells by virtue of their large size, round nucleus, and staggered distribution within the layer. We counted 3,480 HRP-labeled pyramidal cells in layer II. In a second cat, tissue was prepared by cresyl violet staining. We counted 3,676 large cells residing in layer II that were identified as pyramidal cells because they also exhibited smooth round nuclei and prominent Nissl bodies.

DISCUSSION

The purpose of this study was to describe the projections and quantify the terminal arborizations of type I auditory nerve fibers along the tonotopic axis of the DCN. The analysis is based on the complete reconstructions of individual axons and the mapping of their terminal arborizations

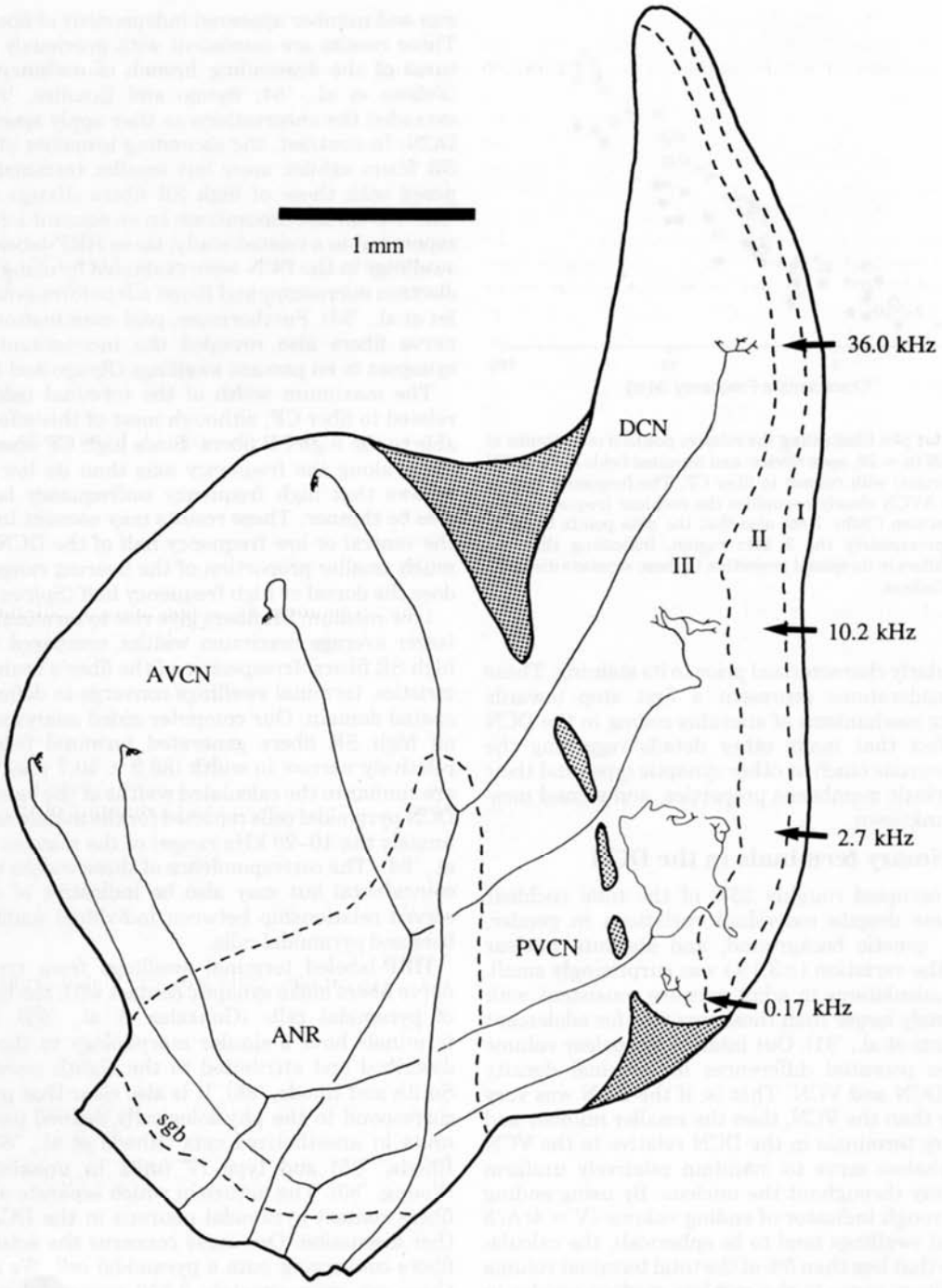

Fig. 10. Drawing tube reconstruction of four HRP-labeled auditory nerve fibers from a single cat. The ascending, descending, and root branches, the endbulbs of Held in the AVCN, and the terminal arborization in the DCN are illustrated for each fiber. The nuclear silhouette is outlined as viewed from a plane parallel to the lateral surface of the nucleus, with anterior to the left and dorsal is up. The CF of each fiber is indicated, as are the DCN layers. The granule cell zone separating the DCN from the VCN is illustrated in stipple. Note the topographic distribution and orientation of the projections in layer III. ANR, auditory nerve root; AVCN, anteroventral cochlear nucleus; DCN, dorsal cochlear nucleus; PVCN, posteroventral cochlear nucleus; sgb, Schwann-glia border.

in three dimensions within the DCN. These data confirm previously published population observations and extend our knowledge of auditory nerve input to the cochlear nucleus at the single fiber level. The morphological data are then considered with respect to the physiological properties of the possible target neurons in the DCN since each fiber

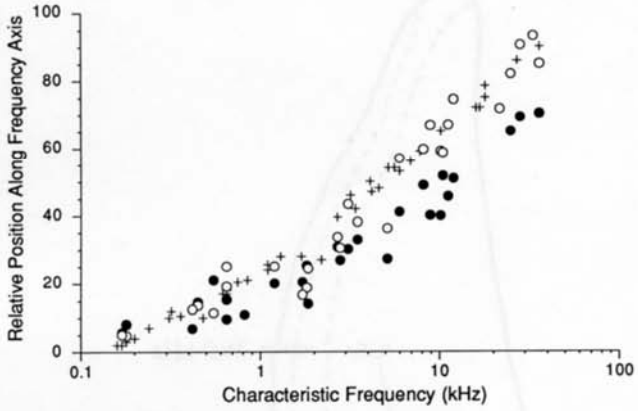

Fig. 11. Scatter plot illustrating the relative position of endbulbs of Held in the AVCN (n = 28, open circles) and terminal fields in the DCN (n = 27, filled circles) with respect to fiber CF. The frequency map of endbulbs in the AVCN closely resembles the cochlear frequency map (crosses) of Liberman ('82b). Note also that the data points begin to separate at approximately the 3 kHz region, indicating that the auditory nerve differs in its spatial projection to these separate divisions of the cochlear nucleus.

was intracellularly characterized prior to its staining. These kinds of considerations represent a first step towards understanding mechanisms of stimulus coding in the DCN despite the fact that many other details regarding the constituent neurons (such as other synaptic types and their locations, intrinsic membrane properties, and second messengers) are unknown.

Primary terminals in the DCN

The DCN occupied roughly 25% of the total cochlear nucleus volume despite individual variations in gender, body weight, genetic background, and absolute nuclear volume, and the variation (±3.1%) was surprisingly small. Our volume calculations in adult cats are consistent with but appropriately larger than those reported for adolescent cats (Hultcrantz et al., '91). Our interest in nuclear volume was to assess potential differences in terminal density between the DCN and VCN. That is, if the DCN was very much smaller than the VCN, then the smaller number and size of primary terminals in the DCN relative to the VCN might nevertheless serve to maintain relatively uniform synaptic density throughout the nucleus. By using ending area (A) as a rough indicator of ending volume ($V = 4rA/3$ since terminal swellings tend to be spherical), the calculations indicate that less than 5% of the total terminal volume from the auditory nerve to the cochlear nucleus resides in the DCN. This projection is proportionally even smaller than the volume difference between DCN and VCN, and is consistent with the observation that cochlear destruction does not affect single unit spontaneous activity in the DCN (Koerber et al., '66). Nonprimary inputs to the DCN or intrinsic cellular mechanisms may endow the nucleus with its basal level of (spontaneous) activity, and removal of the modest primary input is undetectable.

The average size (3.19 ± 2.0 μm^3) and number (12.9 ± 11.0) of terminal swellings per fiber in the DCN is small compared with that in the VCN. Values for terminal size and number appeared independent of fiber CF and SR. These results are consistent with previously reported features of the descending branch of auditory nerve fibers (Fekete et al., '84; Ryugo and Rouiller, '88) and have extended the observations as they apply specifically to the DCN. In contrast, the ascending branches of low-medium SR fibers exhibit more but smaller terminals when compared with those of high SR fibers (Ryugo and Rouiller, '88). We did not concentrate on en passant swellings in this report but in a related study, three HRP-labeled en passant swellings in the DCN were examined by using serial section electron microscopy and found not to form synapses (Gonzalez et al., '93). Furthermore, past examinations of auditory nerve fibers also revealed the inconsistent presence of synapses in en passant swellings (Ryugo and Rouiller, '88).

The maximum width of the terminal field is inversely related to fiber CF, although most of this effect is attributable to the high SR fibers. Since high CF fibers occupy less space along the frequency axis than do low CF fibers, it follows that high frequency isofrequency laminae might also be thinner. These results may account in part for why the ventral or low frequency half of the DCN represents a much smaller proportion of the hearing range in cats than does the dorsal or high frequency half (Spirou et al., '93).

Low-medium SR fibers give rise to terminal fields having larger average maximum widths, compared with those of high SR fibers. Irrespective of the fiber's branching characteristics, terminal swellings converge to define a restricted spatial domain. Our computer-aided analyses suggest that all high SR fibers generated terminal fields that were relatively narrow in width (86.9 ± 40.7 μm). These values are similar to the calculated widths of the basal dendrites of DCN pyramidal cells reported for the middle region (approximately the 10–20 kHz range) of the nucleus (Blackstad et al., '84). The correspondence of these widths may be purely coincidental but may also be indicative of a highly conserved relationship between individual auditory nerve fibers and pyramidal cells.

HRP-labeled terminal swellings from type I auditory nerve fibers make synaptic contact with the basal dendrites of pyramidal cells (Gonzalez et al., '93). Such labeled terminals have a similar morphology to those previously described and attributed to the eighth nerve (Kane, '74; Smith and Rhode, '85). It is also clear that pyramidal cells correspond to the physiologically defined pauser/build-up units in anesthetized cats (Rhode et al., '83; Smith and Rhode, '85) and type IV units in unanesthetized cats (Young, '80). The nature in which separate auditory nerve fibers contact pyramidal neurons in the DCN merits further discussion. One issue concerns the actual number of fibers converging onto a pyramidal cell. We calculate that there are approximately 3,500 pyramidal cells per DCN with a density of approximately nine pyramidal cells per 10^4 μm^2. Given the reported 50,000 fibers in the auditory nerve of cats (Gacek and Rasmussen, '61), and that 85% of them reach the DCN, there are roughly 12 fibers in the DCN for every pyramidal cell. Since the extent of each basal dendrite arborization is on average 80×500 μm (Blackstad et al., '84), a single auditory nerve fiber may contact as few as one, or as many as 36 pyramidal cells. In any case, although the amount of terminal volume (inferred to reflect synaptic contact) delivered to the DCN is small, the convergence by multiple fibers onto a single neuron might serve to amplify

the input. Such a convergence by high SR, low threshold fibers onto pyramidal cells would contribute to their low acoustic thresholds as determined using electrophysiological techniques (Godfrey et al., '75; Young and Brownell, '76; Rhode et al., '83; Smith and Rhode, '85; Rhode and Smith, '86). Because there does not appear to be a population of high threshold type IV units (Young and Brownell, '76), there probably is not an exclusive projection of the low-medium SR, high threshold auditory nerve fibers to individual pyramidal cells.

Elongated and multipolar cells in layer III are also potential postsynaptic targets of auditory nerve fibers because of their spatial relationships to the terminal arborizations. The elongated cells have the size, shape, and distribution of vertical cells (Osen et al., '90). Multipolar cells exhibit a range of sizes; the large ones that lie in the deep region of layer III correspond to giant cells (Osen, '69). The actual demonstration of synaptic contacts between primary fibers and these cells remains to be determined using electron microscopy.

Local circuit interactions

In the context of the above discussion, it seems that different sets of primary fibers might contact different populations of neurons in the DCN. One possibility is that the low SR, high threshold auditory nerve fibers could selectively contact vertical cells, forming the afferent limb of a neural circuit that centers around the physiologically defined type II units. Type II units tend to be distributed within the deep polymorphic region of the DCN (Young and Voigt, '82), have relatively higher thresholds for sound evoked discharges (Young and Brownell, '76), and exhibit little or no spontaneous activity (Young and Brownell, '76; Young and Voigt, '82; Shofner and Young, '85). Type II units can be antidromically activated by stimulation of the VCN, whereas type IV units are antidromically activated via electrical stimulation of the dorsal acoustic stria (Young, '80). The anatomically defined vertical neurons reside in the deep DCN, give rise to a local circuit axon within the DCN (that may or may not contact a pyramidal cell), and roughly one third of them send a collateral into the tuberculo-ventral tract to reach the VCN (Lorente de No, '81). Neurons whose somata reside in the deep DCN can also be retrogradely labeled following HRP injections into the VCN (Saint Marie et al., '91). Neither type II units (Shofner and Young, '85) nor vertical cells (Osen et al., '90) necessarily represent a homogeneous population, but it seems reasonable to propose that at least some subset of these cells represent the same neuronal population as described by different criteria. Some of the properties of type II units may be accounted for by hypothesizing that they receive their predominant excitatory input from low SR auditory nerve fibers. Type II units certainly resemble low SR fibers in several important ways (Liberman, '78; Young and Voigt, '82), although unlike auditory nerve fibers, they do not respond well to broadband noise stimulation (Young and Brownell, '76).

Implications for frequency organization

Low-medium SR fibers innervate a broader region of the strial axis than do high SR fibers. The consequence of this projection, however, is not immediately obvious because it is not known whether fibers of the different SR groups converge upon the same cells and because broadly tuned units are not typical of the DCN, especially near threshold stimulation. At higher levels of stimulation, the possible broadening of tuning properties in second order units via convergence from fibers of different CFs is complicated by the presence of "tails" of tuning curves. By the time threshold for low-medium SR auditory nerve fibers is reached, the response rate of type IV units is being inhibited, hypothetically by input from type II units (Voigt and Young, '80, '90). Clearly, there remain a number of details left to be determined concerning neuronal circuitry and single unit response properties that might help explain the complex response features of the DCN.

The spatial difference in terminal arborization pattern of low versus high SR fibers might also indicate some important details regarding the nature of isofrequency laminae. By virtue of the broader arborizations generated by each low-medium SR fiber, it might be that such fibers preferentially innervate the edges of an isofrequency lamina, whereas the high SR fibers tend to occupy the "center" of the lamina. Such an organization might establish a functional segregation of units having distinct features within an isofrequency lamina, as has been proposed in the inferior colliculus (Roth et al., '78). Mapping experiments investigating CF and threshold distribution utilizing finer-grain spatial resolution might conceivably resolve this possibility.

Terminal field topography

There was strong conformity with respect to the CF of a fiber and the location of its terminal field within the DCN. Because only one or a few fibers are recovered from any single experiment, it was necessary to normalize data across animals so that quantitative comparisons could be made. The position of 26 terminal fields from 20 cats was mapped onto a standardized DCN and found to vary systematically with fiber CF. Furthermore, the orientation of each terminal field was closely aligned with the cellular striations in layer III. These fibro-neuronal striations appear to form the morphologic substrate for the physiologically defined frequency organization (Rose et al., '59; Blackstad et al., '84; Spirou et al., '93).

The systematic mapping of frequency from the organ of Corti to the cochlear nucleus exhibited a pattern of divergence when comparing the projection with the AVCN versus the DCN (Fig. 11). That is, the normalized projection of auditory nerve fibers into the AVCN closely resembles the cochlear frequency map (Liberman, '82b), but there is divergence of the normalized projection of primary fibers into the DCN at about the 3 kHz region. This spatial difference in the relative frequency representation when comparing the cochlea and the DCN may be due in part to the progressively lower innervation density under inner hair cells more apical to the 3 kHz region of the cochlea (Liberman et al., '90). In any case, the primary projection to the AVCN preserves the relative spatial representation of frequency information that is established in the cochlea, whereas the projection to the DCN compresses the representation of low frequency information and expands the representation of high frequencies. The functional significance of this difference remains to be determined.

ACKNOWLEDGMENTS

This project was supported in part by NIH grant DC00232. Some of the experiments were initiated while the authors were members of the Department of Anatomy and Cell Biology, Harvard Medical School, and Eaton-Peabody Lab, Mass. Eye and Ear Infirmary. We thank Tan Pongstaporn and Denise Vause for their technical assistance, and Dr. Brad May and Dr. George Spirou for their critical comments on this manuscript.

LITERATURE CITED

Abercrombie, M. (1946) Estimation of nuclear population from microtome sections. Anat. Rec. *94:*239–247.

Adams, J.C., and W.B. Warr (1976) Origins of axons in the cat's acoustic striae determined by injection of horseradish peroxidase into severed tracts. J. Comp. Neurol. *170:*107–121.

Blackstad, T.W., K.K. Osen, and E. Mugnaini (1984) Pyramidal neurones of the dorsal cochlear nucleus: A Golgi and computer reconstruction study in cat. Neuroscience *13:*827–854.

Borg, E. (1973) On the neuronal organization of the acoustic middle ear reflex: A physiological and anatomical study. Brain Res. *49:*101–123.

Brown, M.C., and J.V. Ledwidth, Jr. (1990) Projections of thin (type-II) and thick (type-I) auditory-nerve fibers into the cochlear nucleus of the mouse. Hearing Res. *49:*105–118.

Davis, M., D.S. Gendelman, M.D. Tischler, and G.M. Gendelman (1982) A primary acoustic startle circuit: Lesion and stimulation studies. J. Neuroscience *2:*791–805.

Evans, E.F., and P.G. Nelson (1973) The responses of single neurones in the cochlear nucleus of the cat as a function of their location and the anesthetic state. Exp. Brain Res. *17:*402–427.

Evans, E.F., and A.R. Palmer (1980) Relationship between the dynamic range of cochlear nerve fibers and their spontaneous activity. Exp. Brain Res. *40:*115–118.

Fekete, D.M., E.M. Rouiller, M.C. Liberman, and D.K. Ryugo (1984) The central projections of intracellularly labeled auditory nerve fibers in cats. J. Comp. Neurol. *229:*432–450.

Feng, A.S., and M. Vater (1985) Functional organization of the cochlear nucleus of Rufous horseshoe bats (Rhinolophus rouxi): Frequencies and internal connections are arranged in slabs. J. Comp. Neurol. *235:*529–553.

Gacek, R.R., and G.L. Rasmussen (1961) Fiber Analysis of the statoacoustic nerve of guinea pig, cat and monkey. Anat. Rec. *139:*455–463.

Godfrey, D.A., N.Y.S. Kiang, and B.E. Norris (1975) Single unit activity in the dorsal cochlear nucleus of the cat. J. Comp. Neurol. *162:*269–284.

Goldberg, J.M., and W.E. Brownell (1973) Discharge characteristics of neurons in anteroventral and dorsal cochlear nuclei of cat. Brain Res. *64:*35–54.

Gonzalez, D.L., P.J. Kim, T. Pongstaporn, and D.K. Ryugo (1993) Synapses of the auditory nerve in the dorsal cochlear nucleus of the cat. ARO Abstr. (in press).

Hultcrantz, M., R. Snyder, S. Rebscher, and P. Leake (1991) Effects of neonatal deafening and chronic intracochlear electrical stimulation on the cochlear nucleus in cats. Hearing Res. *54:*272–280.

Kane, E.C. (1974) Synaptic organization in the dorsal cochlear nucleus of the cat: A light and electron microscopic study. J. Comp. Neurol. *155:*301–330.

Kiang, N.Y.S., T. Watanabe, L.C. Thomas, and L.F. Clark (1965) Discharge Patterns of Single Fibers in the Cats Auditory Nerve. Cambridge: MIT Press.

Koerber, K.C., R.R. Pfieffer, W.B. Warr, and N.Y.S. Kiang (1966) Spontaneous spike discharges from single units in the cochlear nucleus after destruction of the cochlea. Exp. Neurol. *16:*119–130.

Leake, P.A., and R.L. Snyder (1989) Topographic organization of the central projections of the spiral ganglion in cats. J. Comp. Neurol. *281:*612–629.

Liberman, M.C. (1978) Auditory-nerve response from cats raised in a low-noise chamber. J. Acoust. Soc. Am. *53:*442–455.

Liberman, M.C. (1982a) Single-neuron labeling in the cat auditory nerve. Science *216:*1239–1241.

Liberman, M.C. (1982b) The cochlear frequency map for the cat: Labeling auditory-nerve fibers of known characteristic frequency. J. Acoust. Soc. Am. *72:*1441–1449.

Liberman, M.C., L.W. Dodds, and S. Pierce (1990) Afferent and efferent innervation of the cat cochlea: Quantitative analysis with light and electron microscopy. J. Comp. Neurol. *301:*443–460.

Lorente de No, R. (1981) The Primary Cochlear Nuclei. New York: Raven Press.

Moore, J.K. (1980) The primate cochlear nuclei: Loss of lamination as a phylogenetic process. J. Comp. Neurol. *193:*609–629.

Moskowitz, N., and J.C. Liu (1972) Central projections of the spiral ganglion of the squirrel monkey. J. Comp. Neurol. *144:*335–344.

Mugnaini, E. (1985) GABA neurons in the superficial layers of the rat dorsal cochlear nucleus: Light and electron microscopic immunocytochemistry. J. Comp. Neurosci. *235:*61–81.

Mugnaini, E., A.S. Berrebi, A.-L. Dahl, and J.I. Morgan (1987) The polypeptide PEP-19 is a marker for Purkinje neurons in cerebellar cortex and cartwheel neurons in the dorsal cochlear nucleus. Arch. Ital. Biol. *126:*41–67.

Mugnaini, E., W.B. Warr, and K.K. Osen (1980) Distribution and light microscopic features of granule cells in the cochlear nuclei of cat, rat, and mouse. J. Comp. Neurol. *191:*581–606.

Noda, Y., and W. Pirsig (1974) Anatomical projection of the cochlea to the cochlear nuclei of the guinea pig. Arch. Oto-Rhino-Laryn. *208:*107–120.

Osen, K.K. (1969) Cytoarchitecture of the cochlear nuclei of the cat. J. Comp. Neurol. *136:*453–484.

Osen, K.K. (1970) Course and termination of the primary afferents in the cochlear nuclei of the cat. Arch. Ital. Biol. *108:*21–51.

Osen, K.K., O.P. Ottersen, and J. Storm-Mathisen (1990) Colocalization of glycine-like and GABA-like immunoreactivities: A semiquantitative study of individual neurons in the dorsal cochlear nucleus of cat. In O.P. Ottersen and J. Storm-Mathisen (eds). *Glycine Neurotransmission,* New York: J. Wiley and Sons, pp. 417–451.

Pfeiffer, R.R. (1966) Classification of response patterns of spike discharges for units in the cochlear nucleus: Tone-burst stimulation. Exp. Brain Res. *1:*220–235.

Ramón y Cajal, S. (1909) Histologie du Systeme nerveux de l'Homme et des Vertebres, Vol 1. Madrid: Instituto Ramon y Cajal, pp. 774–838.

Rhode, W.S., and P.H. Smith (1986) Physiological studies on neurons in the dorsal cochlear nucleus of cat. J. Neurophysiol. *56:*287–307.

Rhode, W.S., P.H. Smith, and D. Oertel (1983) Physiological response properties of cells labeled intracellularly with horseradish peroxidase in cat dorsal cochlear nucleus. J. Comp. Neurol. *213:*426–447.

Rose, J.E., R. Galambos, and J.R. Hughes (1959) Microelectrode studies of the cochlear nuclei of the cat. Bull. Johns Hopkins Hospital *104:*211–251.

Roth, G.L., L.M. Aitkin, R.A. Andersen, and M.M. Merzenich (1978) Some features of the spatial organization of the central nucleus of the inferior colliculus of the cat. J. Comp. Neurol. *182:*661–680.

Rouiller, E.M., R. Cronin-Schreiber, D.M. Fekete, and D.K. Ryugo (1986) The central projections of intracellularly labeled auditory nerve fibers in cats: An analysis of terminal morphology. J. Comp. Neurol. *249:*261–278.

Ryugo, D.K. and E.M. Rouiller (1988) The central projections of intracellularly labeled auditory nerve fibers in cats: Morphometric correlations with physiological properties. J. Comp. Neurol. *271:*130–142.

Ryugo, D.K., and S. Sento (1991) Synaptic connections of the auditory nerve in cats: Relationship between endbulbs of Held and spherical bushy cells. J. Comp. Neurol. *305:*35–48.

Ryugo, D.K., and F.H. Willard (1985) The dorsal cochlear nucleus of the mouse: A light microscopic analysis of neurons that project to the inferior colliculus. J. Comp. Neurol. *242:*381–396.

Saint Marie, R.L., C.G. Benson, E.-M. Ostapoff, and D.K. Morest (1991) Glycine immunoreactive projections from the dorsal to the anteroventral cochlear nucleus. Hearing Res. *51:*11–28.

Sando, I. (1965) The anatomical interrelationships of the cochlear nerve fibers. Acta. Otolaryngol. *59:*417–436.

Shofner, W.P., and E.D. Young (1985) Excitatory/inhibitory response types in the cochlear nucleus: Relationships to discharge patterns and re-

sponses to electrical stimulation of the auditory nerve. J. Neurophysiol. *54*:917–939.

Smith, P.H., and W.S. Rhode (1985) Electron microscopic features of physiologically characterized, HRP-labeled fusiform cells in the cat dorsal cochlear nucleus. J. Comp. Neurol. *237*:127–143.

Spirou, G.A., B.J. May, D.D. Wright, and D.K. Ryugo (1993) Frequency representation in the dorsal cochlear nucleus of cats. J. Comp. Neurol. *329*:36–52.

Voigt, H.F., and E.D. Young (1980) Evidence of inhibitory interactions between neurons in dorsal cochlear nucleus. J. Neurophysiol. *44*:76–96.

Voigt, H.F., and E.D. Young (1990) Cross-correlation analysis of inhibitory interactions in dorsal cochlear nucleus. J. Neurophysiol. *64*:1590–1610.

Warr, W.B. (1982) Parallel ascending pathways from the cochlear nucleus. Contrib. Sens. Physiol. *7*:1–38.

Webster, D.B. (1971) Projection of the cochlea to cochlear nuclei in Merriam's kangaroo rat. J. Comp. Neurol. *143*:323–340.

Wouterlood, F.G., and E. Mugnaini (1984) Cartwheel neurons of the dorsal cochlear nucleus: A Golgi-electron microscopic study in rat. J. Comp. Neurol. *227*:136–157.

Wouterlood, F.G., E. Mugnaini, K.K. Osen, and A.-L. Dahl (1984) Stellate neurons in rat dorsal cochlear nucleus studied with combined Golgi impregnation and electron microscopy: synaptic connections and mutual coupling by gap junctions. J. Neurocytol. *13*:639–664.

Young, E.D. (1980) Identification of response properties of ascending axons from dorsal cochlear nucleus. Brain Res. *200*:23–37.

Young, E.D., and W.E. Brownell (1976) Responses to tones and noise of single cells in dorsal cochlear nucleus of unanesthetized cats. J. Neurophysiol. *39*:282–300.

Young, E.D., W.P. Shofner, J.A. White, J.-M. Robert, and H.F. Voigt (1988) Response properties of cochlear nucleus neurons in relationship to physiological mechanisms. In G.M. Edelman, W.E. Gall, and W.M. Cowan (eds): Auditory Function. New York: John Wiley and Sons, pp. 277–312.

Young, E.D., and H.F. Voigt (1982) Response properties of type II and type III units in dorsal cochlear nucleus. Hearing Res. *6*:153–169.